ACS Catalysis

pubs.acs.org/acscatalysis
Research Article

Systematic Exploration of a Multi-Promoter Catalyst Composition Space with Limited Experiments: Non-Oxidative Propane Dehydrogenation to Propylene

Christian Kunkel, Frederik Rüther, Frederic Felsen, Charles W. P. Pare, Aybike Terzi, Robert Baumgarten, Esteban Gioria, Raoul Naumann d'Alnoncourt, Christoph Scheurer, Frank Rosowski,* and Karsten Reuter*

Cite This: ACS Catal. 2024, 14, 9008−9017

Read Online

ACCESS | Metrics & More | Article Recommendations | Supporting Information

ABSTRACT: Promoters are indispensable for the optimized performance and lifetime of industrial catalysts. Present-day systems nevertheless benefit only from a small number of different promoters, identified and often only locally optimized in laborious empirical research. Here, we present an accelerated discovery approach that globally explores a multipromoter design space with only limited experiments. Cornerstones are an efficient iterative design-of-experiment (DoE) planning of the measurements and a throughput maximization through a parallelized testing protocol. With less than 100 experiments conducted within weeks, we identify a competitive promoter chemistry for the nonoxidative propane dehydrogenation to propylene over alumina-supported Pt. This discovery rests on an achieved deep understanding of the positive and negative actions of multiple promoters on the reaction yield and deactivation. The iterative DoE strategy successively querying batches of experiments proves to be a powerful general concept for data-efficient hypothesis validation and insight-based adaptation of design spaces.

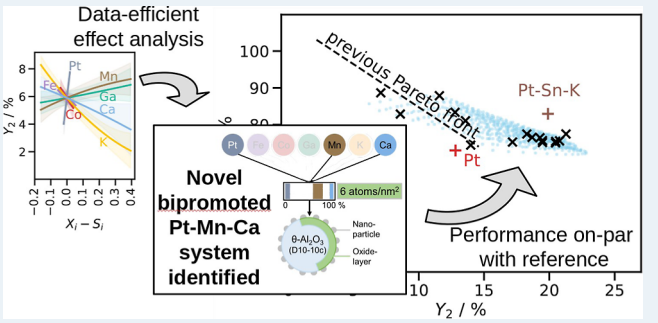

KEYWORDS: *high-throughput experimentation, automated laboratory, design of experiment, active learning, non-oxidative propane dehydrogenation, heterogeneous catalysis, promoters*

INTRODUCTION

Promoters are a prevalent ingredient to industrial catalysis, enhancing performance, improving selectivity, or mitigating deactivation.[1−4] Various modes of action are known, such as modifying the electronic structure, facilitating reactant adsorption, or favoring specific reaction pathways.[5−8] These actions extend over both the active material and the support[9,10] and depend sensitively on both type and concentration of the employed promoter(s). Lacking a full mechanistic understanding of these complex actions, the additive selection of suitable promoters and simultaneous optimization of concentrations are, in practice, a time-consuming empirical endeavor. Rather than systematically exploiting the full combinatorial multipromoter design space, industrial catalyst systems therefore typically feature only one or two promoters, at concentrations that are only locally optimized. Due to limited experimental budgets, the optimization is often even carried out sequentially, i.e., the first promoter concentration is varied around the optimized unpromoted system, the second promoter concentration then varied around the thus "optimized" one-promoter system, and so forth.

The nonoxidative propane dehydrogenation (PDH) to propylene is a prime example for this common situation. As one of the most important feedstock chemicals, e.g., polymer manufacturing, propylene demand is expected to approach 200 megatons by 2030,[11] which cannot be met with the existing cracking processes.[12] Industrial scale catalysts for the PDH reaction usually build on oxidic support materials with ≤1 wt % Pt or 18−20 wt % CrO_x as active metals.[10,13] With the large-scale application in mind, high surface area alumina (Al_2O_3) is a preferred support choice following its thermal and mechanical stability and comparably high density.[13] Unfortunately, the process suffers from side reactions toward lower alkanes, as well as severe coke formation, which leads to a fast deactivation of the catalyst under operation conditions.[11,14,15] A working process therefore often incorporates regular

Received: March 21, 2024
Revised: May 17, 2024
Accepted: May 17, 2024
Published: May 29, 2024

regeneration steps to remove the formed coke and restore the initial activity of the catalytic system—up to a point, where irreversible long-term deactivation (due to persistent sintering) poses a challenge. To improve on this situation, a variety of promoters have been studied with the goal to maximize product yields or the overall efficiency of the process.[12,13,16] A now commercially applied process (Oleflex) comprises the ternary catalyst formulation Pt−Sn−K that emerged from such studies throughout the last decades.[17−19] Indeed, more than 40 (!) years passed from the finding of Pt to be active in the dehydrogenation of paraffins,[20−22] over first investigations on the promoting effect of Sn,[17] to the first industrial application starting from paraffins (Pacol-process),[23] and finally the development of the Oleflex process.

Even so, not even this process achieves to push the yield limitations of this system toward an operation at the thermodynamic limit.[12] In order to ultimately achieve this ambitious goal, the identification of new high-performance multipromoter combinations and a deeper chemical understanding of the promoting effects are considered as key factors.[12,16,24] Ideally, such promoters also suppress the challenging reversible fast deactivation of the catalysts, leading to a smart process that relies on fewer regeneration steps or, in the ideal case, results in a continuous process without regeneration at all. Here, we address this with an accelerated discovery approach for complex multipromoted systems. This approach systematically explores the corresponding high-dimensional design space spanned by the employed promoter species and their concentrations. Central pillars are efficient experiment planning based on an iterative design of experiment (DoE) approach as well as an experiment setup that holistically considers the entire workflow from synthesis to catalytic testing. The prior planning enables systematic promoter space exploration at a number of samples explicitly to be studied that is comparable to previous local and sequential optimizations. The latter experiment setup then maximizes the throughput of these studies by automating and efficiently parallelizing the limiting steps in the workflow, e.g., through a dedicated time-resolved testing protocol for a multireactor setup. At restricted human intervention, the complete synthesis-to-testing for a batch of eight samples can thus be achieved every 5 days.

We initially minimize an interfering influence of free support sites and analyze the action of six potential promoters (Fe, Co, Ga, Mn, K, and Ca; see below) on the PDH at Pt on $\theta - Al_2O_3$ in the limit of surface-covering promotion. The global view of this multipromoter design space reached after testing only five batches reveals a Pareto front between the two central performance descriptors, propylene yield and fast deactivation. Subsequent batches designed to specifically assess the separate actions of the promoters trace this Pareto dilemma down to the individual promoter level. An improvement in one performance descriptor brought about by the addition of any promoter always comes at the cost of a deterioration in the other descriptor, and there are no significant multipromoter interactions that would allow to overcome this limitation. Intriguingly, the six promoters fall into two groups with similar actions though. While one group improves product yield at increased fast deactivation, the other group reduces deactivation at reduced product yield. Naturally, best compromise performance gains can therefore be obtained at the boundaries of the design space, where at a reduced number of different promoters, optimally tuned concentrations of ultimately only one representative of each promoter group allow to maximally compensate these opposing actions. Leveraging this deep understanding, we therefore switch to a lower-dimensional design space, where we only retain a most promising promoter of each group and finally explore additional support site effects by allowing for total concentrations below the surface-coverage promotion limit. The global view of this bipromoted (Mn and Ca)-space reached after only two further batches shows that the intrinsic support activity essentially only shifts the Pareto front. It does it to such an extent though that a performance comparable to the established Pt−Sn−K reference can be reached. With only a very limited number of experiments performed within a matter of weeks, our accelerated discovery approach thus rationally leads to a new promoter formulation that is competitive to the one arrived at over decades of empirical research.

RESULTS

Delineation of the Multipromoter Design Space. In the selection of the six promoter species investigated in our approach, we can draw on an ever increasing variety of single-promoter studies of Pt-based PDH catalysts in literature.[12,13] The reported elements with a potentially beneficial effect on the catalysis are alkali and earth-alkali metals like K or Ca, 3d transition metals like Mn, Fe, or Co, as well as main group metals like Al, Ga, or Sn. The increased selectivities observed upon the addition of alkali or earth-alkali metals are thereby mainly assigned to their potential to moderate the strong acid sites of the Al_2O_3 support.[9,16,25−30] In contrast, the promoting effect of the metals is more discussed in terms of an improved Pt dispersion[31−34] or the formation of intermetallic or oxidic compounds.[6,7,12,35−41] Aiming to cover all of these suspected actions, we select two likely reducible (Fe, Co), two hardly reducible (Ga, Mn), and two moderating elements (K, Ca) as the promoters spanning the design space for a multipromoter PDH system. From the two known Oleflex promoters (Sn and K), the function of Sn is quite well understood in terms of Pt/Sn nanoalloy or intermetallic formation. We therefore deliberately excluded it from our study in favor of less well-known promoters that also might form alloys. The role of K, on the other hand, is less clear. Reports on its moderation of the acidity of the alumina support consider only the lowest concentrations. We therefore deliberately kept K in the study to see if it has an additional effect if the concentration exceeds the threshold needed for the moderation of acid sites. Independent of this selection, we still use a Pt−Sn−K formulation with concentrations mimicking the Oleflex system as a benchmark catalyst to put the observed catalytic performances to scale; see experimental section and the Supporting Information for more details.

Pt and the promoters are applied to the thermally pretreated $\theta - Al_2O_3$ support by incipient wetness impregnation. With the objective to first analyze the Pt-promoter interactions at minimized additional interactions with free support sites, we pursue a surface-covering promotion concept and only consider catalysts where the total loading of Pt and all promoters arithmetically equals about one monolayer on the surface of the support (determined to amount to 6 atoms per nm^2; see Supporting Information). Henceforth, we report the respective surface concentrations X_i (i = Pt, Fe, Co, Ga, Mn, K, and Ca) as fractions of this targeted total surface concentration. We then have $\sum_i X_i = 1.0$ and the conversion to nominal weight loadings is provided in Table S1. For Pt, we investigate an economically viable range of $0.02 \leq X_{Pt} \leq 0.06$,

https://doi.org/10.1021/acscatal.4c01740
ACS Catal. 2024, 14, 9008−9017

amounting to nominal Pt loadings between 0.10 and 0.29 wt %. As pre-experiments indicated excessive coke formation and reactor blocking, the maximum surface fractions of Fe and Co need to be limited to 0.1, with an additionally imposed multicomponent constraint $X_{Fe} + X_{Co} \leq 4 \cdot X_{Pt}$. At the same time, we suspect nontrivial performance variations in the limit of individually vanishing promoter concentrations. To ensure a sufficient smoothness for the intended DoE-based exploration of the design space, we therefore also set minimum surface fractions of 0.02 for Fe and Co and 0.05 for all other promoters. In consequence, this defines maximum concentrations for Ga, Mn, K, and Ca of 0.75.

Experiment Planning. Even though we formally vary the concentrations of Pt and all six promoters, the mixture constraint ($\sum_i X_i = 1.0$) reduces this to a six-dimensional design space.[42,43] Due to uncertainty in the experimental synthesis, only variations with a minimum change of surface fractions will reliably yield a new catalyst. If we loosely use 0.02 (0.05) as this minimum step size for Pt, Fe, and Co (Ga, Mn, K, and Ca) and account for the above-mentioned multicomponent constraint for $X_{Fe} + X_{Co}$, this leads to a total of 7265 unique catalysts that can in principle be synthesized in the defined design space. While not excessively large in absolute numbers, mapping this space exhaustively is essentially not tractable. Even in the parallel experiment setup further detailed below with a throughput of eight samples per 5 days, this would amount to a continuous experimentation over more than 12 years. We therefore follow a DoE philosophy to determine the response surface in terms of propylene yield and deactivation over the design space from a set of carefully planned measurements.

For an initial exploration that avoids an overly reliance on assumptions like a smoothly varying response surface or the absence of significant promoter interactions, we first developed a problem adapted screening, addressing at the same time blocking and mixing constraints, that yields a space-filling distribution of 35 catalyst compositions. This algorithm first constructs a space-filling mixture design of 27 compositions with an ensured minimum separation between the two points. Eight additional compositions are then purpose-selectedly added after analysis of this initial distribution. Nine randomly selected compositions from this design are replicated, either fully resynthesized and tested or retested in a different reactor tube. Together with 12 reference measurements (blind test, unpromoted Pt, only promoters, bare support, Pt−Sn−K, also replicated), this yields a total of 56 samples that are measured in seven batches. Full details on the design construction are given in the Supporting Information, and the full design, replications, and references are reproduced in Tables S4−S7.

Time-Efficient Parallel Catalytic Testing. Catalyst testing focuses on the reaction yield $Y_{propylene}$, as a combination of the conversion of propane in a continuous flow system and product selectivity. For the very dynamic PDH reaction, which shows a fast (reversible) deactivation over time, we specifically measure the transient behavior of $Y_{propylene}$ over two PDH cycles with a time on stream (TOS) of 24 h each and a 2 h regeneration phase using a stepped oxygen supply in between. Figure 1 shows a corresponding trace for an unpromoted Pt reference catalyst with a 0.06 surface fraction (0.29 wt % loading). The strong transient in particular in the initial formation phase with high conversion at limited selectivity challenges an efficient parallel testing. The need to resolve this transient in short time steps clashes with the intrinsic time

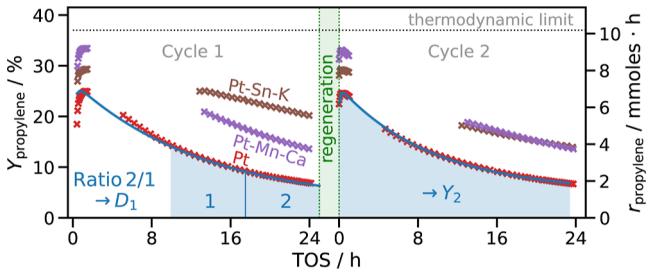

Figure 1. Extraction of catalytic performance descriptors from measured reaction yield traces. The reaction yield toward propylene is shown over two PDH cycles of 24 h each with a 2 h regeneration period in between (to restore the diminished activity after the fast deactivation in the initial cycle). For clarity, the propylene formation rate $r_{propylene}$ [mmol/h] (right y-axis) is normalized to reaction yield Y in % of the amount of propane dosed per time (left y-axis). Shown are data for an unpromoted Pt reference catalyst (X_{Pt} = 0.06), for a Pt−Sn−K reference catalyst (X_{Pt} = 0.09, X_{Sn} = 0.07, X_K = 0.52, cf. Supporting Information for details), and for a here identified Pt−Mn−Ca catalyst (X_{Pt} = 0.04, X_{Mn} = 0.25, X_{Ca} = 0.25); see text. The dotted horizontal line marks the thermodynamic limit for the reaction yield. Integration of the fitted interpolation function (blue line) over the 24 h TOS of each cycle i yields the integral yield descriptor Y_i for propylene (in % of the total amount of propane dosed over the same period of time). The descriptor D_i for the fast deactivation over each cycle results from the fraction of the integrated subtraces in the time windows [17.5 h; 25 h] and [10 h; 17.5 h]. The missing data ranges result from the parallel testing protocol described in the main text.

demand of the gas analysis through gas chromatography (GC). Even a highly optimized GC-measurement with a simple separation task including C1 to C4 alkanes and olefins still takes around ∼4 min. Simply alternating these measurements between the eight tubes in our parallel reactor setup would then only yield data in ∼32 min steps.

We therefore develop a time-resolved parallel testing (TRPT) protocol fully described in the Supporting Information, in which the testing in the different reactor tubes starts subsequently, each with a 1 h delay. This way, the first reactor is heated to reaction temperature and the transient behavior of the PDH catalyst can be monitored at high resolution, while all other reactors are still inactive. After 1 h, the second reactor is heated and this sample is exclusively tested for 1 h. This procedure is continued until all reactors are at reaction temperature. From then on, all reactors are monitored with alternating GC-measurements at a concomitant lower resolution. However, at these later times, the deactivation, then primarily through coking and sintering, also proceeds on longer time scales, which do not need such a high resolution; cf. Figure 1. The smoothness of $Y_{propylene}$ at this later TOS also mitigates the measurement break that necessarily results from the TRPT, where the first seven reactors are not tested for a certain period of time after they have already reached the reaction temperature.

We can therefore robustly fit the TOS data of each cycle with a simple sum of two exponentially decaying functions, as motivated by the two deactivation regimes. As illustrated in Figure 1, integrating this function over each cycle then yields Y_1 and Y_2 as a meaningful descriptor for the integral yield in the main product propylene. In order to also capture the fast deactivation behavior, we additionally define a second descriptor $D_{1/2} = Y_{1/2}^{[17.5h;25h]}/Y_{1/2}^{[10h;17.5h]}$ as the ratio of the integral yields of the subtraces over the time range from 17.5 to 25 h and 10 to 17.5 h; see Supporting Information for full

https://doi.org/10.1021/acscatal.4c01740
ACS Catal. 2024, 14, 9008−9017

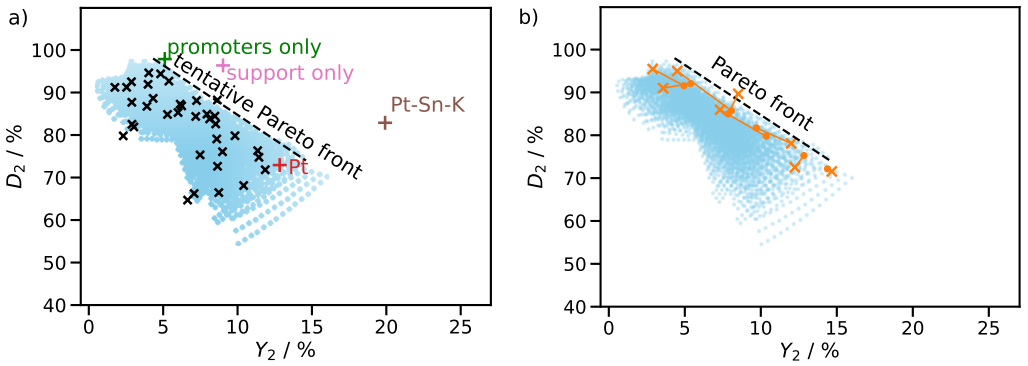

Figure 2. Overview over the multipromoter catalyst design space. (a) Performance descriptors for reaction yield Y_2 and deactivation D_2 for the 7265 unique catalysts in the design space as predicted by the regression model (blue dots). The descriptors for the 35 explicitly measured compositions are shown as black crosses. Also shown are the descriptors for the unpromoted Pt catalyst (red cross) and the Pt−Sn−K reference catalyst (brown cross) already discussed in Figure 1, as well as for the empty support (pink cross) and a support largely covered with promoters only (green cross, $X_{Fe/Co} = 0.08$, $X_{Ga/Mn/K/Ca} = 0.2$); see text. (b) Same as (a), but including the data for an additional batch of eight experiments to validate the Pareto front apparent from the model prediction. Orange dots are the model predictions, orange crosses the subsequently measured corresponding experimental values.

details of the descriptor definitions as well as of a series of dedicated replication experiments that confirm a replication accuracy (root-mean-square error) of ±0.5/0.7% in $Y_{1/2}$ and of ±2.2/2.8% in $D_{1/2}$. High $Y_{1/2}$ and high $D_{1/2}$ values are thus favorable, encoding catalysts with a high product yield and slow deactivation. We specifically employ Y_2 and D_2 of the second cycle as the DoE response functions, as we expect the performance over the second PDH cycle to be more representative for the longer term catalyst function. As apparent from Figure 1, the Pt−Sn−K reference catalyst indeed significantly improves over the unpromoted Pt catalyst, with respect to both descriptors. The reaction yield is much higher and the rate of deactivation is decreased.

Global Exploration of the Design Space. We already achieve high-quality fits of the measured response data $Y_{2,j}$ and $D_{2,j}$ for the j = 1, ..., 35 catalyst compositions of our space-filling design with Scheffé-form linear models appropriate for mixture constraints[44]

$$Y_{2,j} = \beta_{Pt}X_{Pt,j} + \beta_{Fe}X_{Fe,j} + \beta_{Co}X_{Co,j} + \beta_{Ga}X_{Ga,j} + \beta_{Mn}X_{Mn,j} + \beta_{K}X_{K,j} + \beta_{Ca}X_{Ca,j} \quad (1)$$

with the fit parameters $\beta_{Pt/Fe/Co/Ga/Mn/K/Ca}$ and an analogue model for $D_{2,j}$. These models can be further improved by adding the most decisive blending terms $\beta_{xy}X_{x,j}X_{y,j}$ among the seven considered elements (Pt and six promoters). The latter is motivated from a chemical perspective, as pairwise interactions might occur between a few but likely not all of the incorporated elements. Specifically, we compute the 10 most promising models for each response, when allowing up to 3 blending terms to be added, and finally obtain robust predictions for Y_2 and D_2 by averaging over the 10 model predictions. Full details of the models and the fitting procedure are given in the Supporting Information. The predictive quality of the models is reflected in a low root-mean-square error of 0.8 (2.9)% for Y_2 (D_2).

On the basis of the established model, Figure 2a provides an overview over the performance descriptors of all 7265 unique catalysts in the design space. The 35 explicitly measured compositions are highlighted and distribute over a large part of the range of achievable descriptors. This confirms the original space-filling design concept and suggests that the model predictions are largely based on interpolation. Unfortunately, the achieved global overview over the possibilities in the considered multipromoter design space indicates a Pareto front between reaction yield and deactivation. More active catalysts (higher Y_2) deactivate faster (lower D_2). This also holds for the unpromoted Pt reference catalyst and the empty support, the data of which are also included in Figure 2a. The empty support is, of course, less active but barely deactivates over the cycle. Intriguingly, however, this product yield of the empty support is nevertheless actually far from being zero; i.e., the support exhibits a significant intrinsic activity. This contribution is obviously suppressed in the present limit of surface-covering promotion, as illustrated by the reduced Y_2 performance descriptor of a representative promotor-only reference catalyst with nearly full surface coverage also included in Figure 2a.

According to the model and in the considered range of concentrations, none of the tested promoter combinations is thus able to break the yield-deactivation trade-off suspected from single-promoter studies.[13,16,45,46] In order to validate this important but slightly disappointing insight, we devise a further batch of experiments to specifically probe the tentative Pareto front. On the basis of the predicted performance descriptors, eight compositions are chosen accordingly, cf. Supporting Information, with Figure 2b displaying their location all along the Pareto front. Figure 2b also shows their performance descriptors that are subsequently obtained in the measurements. While there are in part significant deviations between predicted and measured performance, the overall insight into the existence of a Pareto front is fully confirmed.

Unfortunately, in the present surface-covering promotion limit, this Pareto front runs at quite some distance from the established Pt−Sn−K reference catalyst, cf. Figure 2a. While the considered promoters can drastically slow down deactivation, with D_2 values equal to or substantially higher than the one of the Pt−Sn−K catalyst, this comes at the prize of a strongly reduced yield. Indeed, the largest fraction of all 7265 multipromoted catalysts is in fact predicted to have substantially higher D_2 descriptors than the unpromoted Pt reference catalyst. Instead, very few are predicted to exhibit higher yields. Ascribing the latter mostly to the lacking yield contribution from empty support sites, it is thus imperative to

https://doi.org/10.1021/acscatal.4c01740
ACS Catal. 2024, 14, 9008−9017

evaluate the action of the individual promoters and identify those with the strongest effects per concentration. These promoters would then be prime candidates for a low surface-covering promoter formulation, i.e., a formulation that achieves a slowed down deactivation similar to those in Figure 2a, while simultaneously blocking only a minimum number of support sites.

Analyzing Individual Promoter Effects. Figure 3 shows the variation of the two primary descriptors Y_2 and D_2 along

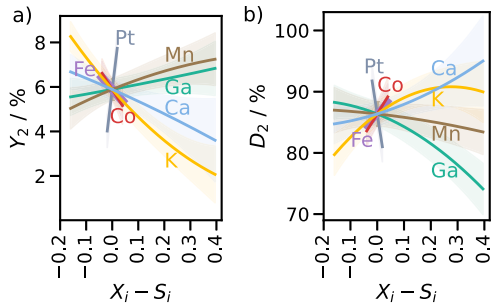

Figure 3. Individual promoter effects. Main effects of Pt and the six promoters on (a) reaction yield descriptor Y_2 and (b) deactivation descriptor D_2. Within the given mixture constraints, these individual effects are approximately obtained along Cox directions varying the surface fraction X_i of the corresponding component around a reference point S_i (X_{Pt} = 0.04, $X_{Fe/Co}$ = 0.06, $X_{Ga/Mn/K/Ca}$ = 0.21) in the middle of the design space, while making appropriate compensating changes to the other surface fractions; see text. Confidence intervals at the 95% level around each predicted mean effect are provided with a lighter transparent shading.

Cox component effect directions[42,47] for Pt and the six promoters. In an independent factor experiment, the main effect of one promoter would be assessed by varying its surface fraction, while keeping all other components unchanged. Within a mixture constraint, components cannot be varied independently of each other though. Cox component effect directions are then a good approximation of an independent one-factor variation by making appropriate changes to the other components that lead to minimum aliasing. Full details on the construction of the Cox directions around a reference point S in the center of the design space, as well as an explicit experimental validation of the deduced effects are given in the Supporting Information. Note in particular that here and henceforth we exploit the availability of the eight additional experimental measurements done to analyze the Pareto front above and refit the DoE-based predictive model to the accordingly enlarged experimental database of 43 compositions. The predictive quality of the models is again reflected in a low root-mean-square error of 1.1 (3.3)% for Y_2 (D_2).

The main effect of the active metal Pt seen in Figure 3 is as intuitively expected. More Pt leads to an increase in the reaction yield at a concomitantly increasing deactivation. Unfortunately, an analogue yield-deactivation trade-off is individually observed for all investigated promoters, too. An improvement in one performance descriptor always comes at the cost of deterioration in the other. Intriguingly, however, the promoters are separated into two classes. An increasing fraction of Ga or Mn leads to an increase in reaction yield, at a simultaneous decrease of D_2. In contrast, the addition of all other promoters (Fe, Co, Ca, and K) stabilizes the system with increasing D_2, while reducing the reaction yield.

Overall, these different actions are fully consistent with previous qualitative assignments from single-promoter studies in literature.[27,29,31,35,36,38] However, our present quantitative analysis in the full multipromoter space reveals quite pronounced differences in the magnitude of the effects. In particular, already smallest changes of the Fe or Co fractions have drastic effects on both Y_2 and D_2, cf. their steep slopes shown in Figure 3, whereas all other promoters have a much weaker effect. Interestingly, the magnitude of the effect on one performance descriptor can also be quite different from that on the other one. The moderate beneficial effect of more Ga on the reaction yield is, for example, accompanied by a dramatic reduction of D_2. In this respect, Mn is a much more promising promoter. It achieves an even slightly higher increase of Y_2 as Ga, but it worsens the deactivation behavior much less. A similar case can be observed in the other promoter group that slows deactivation with increasing D_2 at higher fractions. Here, Ca and K lead to similar D_2 increases, but Ca reduces the reaction yield much less.

Insight-Guided Extension of the Design Space. In particular the identified opposing actions of the two groups of promoters underscore the hitherto barely exploited potential of multipromoter systems, where in an optimum mixture the unavoidable deteriorating effects of promoter(s) of one group are maximally compensated by the beneficial action of promoter(s) of the other group. At the varying strengths of actions apparent in Figure 3, this compensation could also be achieved at quite differing concentrations. A small surface fraction of a strongly acting promoter may then compensate the effect of a larger surface fraction of a weakly acting promoter. At the same time, similar actions of the various promoters within one group identified above question the minimum concentrations we initially imposed for each promoter in the mixture constraint. While the latter allowed to establish a reliable DoE model for a first overview and the present analysis, precisely this analysis now suggests an extension of the design space to where individual promoter concentrations go down to zero. This way, a minimum presence of promoters whose action is equally achieved by another promoter is not unnecessarily enforced, while at the same time, higher maximum surface fractions of other promoters can be explored under the given mixture constraint. Seeing the beneficial action, in particular, of Mn on the reaction yield, one hope is that such higher maximum fractions in a concomitantly extended design space could particularly improve the reachable performance descriptors toward Y_2 that are more competitive with the Pt−Sn−K reference catalyst.

We correspondingly set the lowest possible surface fraction for all promoters to 0.0 and concomitantly increase the maximum possible fractions of Ga, Mn, K, and Ca to 0.9. Under the given mixture constraint and the same step widths in fractions as before, this leads to an increased design space comprising 19,836 unique catalysts. Figure 4 summarizes the performance descriptors predicted by the regression model for this extended space. The range of predicted performance descriptors in Figure 4 is now significantly increased, confirming the expectations from the effect analysis, and extends in particular to much higher reaction yields.

A Pareto front is still visible. However, in particular toward larger Y_2, this front changes slope and less deactivation occurs upon increased reaction yield. This thus improves upon the originally deduced Pareto front in the smaller design space and already reduces the performance gap to the Pt−Sn−K catalyst.

https://doi.org/10.1021/acscatal.4c01740
ACS Catal. 2024, 14, 9008−9017

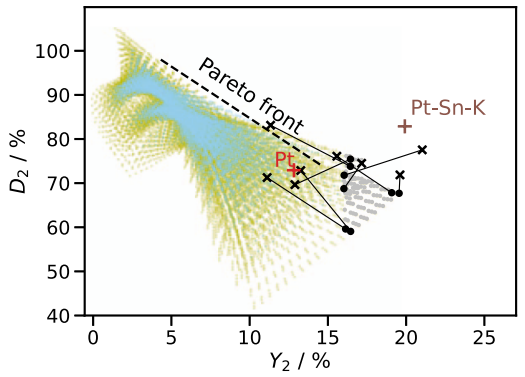

Figure 4. Identification of higher yield catalysts in an extended design space. Performance descriptors for reaction yield Y_2 and deactivation D_2 as predicted by the regression model for 19 836 unique catalysts in an extended design space that allows individual promoter concentrations to go to zero (olive dots), while maintaining the surface-covering promotion limit; see text. Additionally shown are the 7265 unique catalysts in the original design space summarized already in Figure 2 (blue dots), the Pareto front deduced from these original data, as well as the descriptors for the unpromoted Pt catalyst (red cross) and the Pt−Sn−K reference catalyst (brown cross). Eight promising compositions are suitably chosen (black dots) from the top 100 candidates (gray dots) with highest Y_2 in this extended design space. Their subsequently measured corresponding experimental values are shown as black crosses.

We have to recognize though that the model predictions in this rightmost part of the Pareto front in Figure 4 are likely less reliable. The corresponding catalyst compositions are at the outer boundary of the design space, where deviations from the simple behavior assumed in our DoE model are to be expected. To assess the corresponding uncertainty in the predicted position of the Pareto front, we subjected a series of promising candidate compositions with highest predicted Y_2 to experimental testing. Specifically and using a space-filling algorithm analogous to the one employed for the initial exploration of the design space, cf. Supporting Information for details, we choose a batch of eight candidates from the pool of 100 such highest predicted-yield compositions. This pool, the selected batch, and the outcome of the measurements are also displayed in Figure 4. As expected, the actually measured performance descriptors do vary quite a bit from the predictions. Notwithstanding, half of the candidates from the batch indeed exhibit reaction yields that are significantly larger than the one of the Pt reference catalyst. This confirms the understanding that higher Y_2 values are possible at the boundaries of the now enlarged design space. In fact, two of the measured candidates even show yields that are comparable to the one of the Pt−Sn−K reference catalyst (Y_2s of 19.6 and 21.0 vs 19.9%, respectively). Unsurprising from the perspective of the effect analysis, they contain essentially either only Mn or Mn and Ca.

Support Site Effects in the (Pt, Mn, and Ca) Space. The understanding gained so far separates the six promoters into two groups of similar actions, underscores the necessity to go up to higher surface concentrations in individual promoters, and motivates lower surface-covering formulations that then allow for the additional yield contribution from empty support sites. In a final step, we implement this understanding by switching to the low-dimensional (Pt, Mn, and Ca) design space, in which we give up the mixture constraint and consider any total concentrations up to full surface coverage. With Mn and Ca, this retains the most promising promoter from each group, according to the effect analysis. Relying on the previously introduced space-filling algorithm, we design two batches of measurements to determine a polynomial model with full details provided in the Supporting Information. Figure 5 shows the performance descriptors of these measured

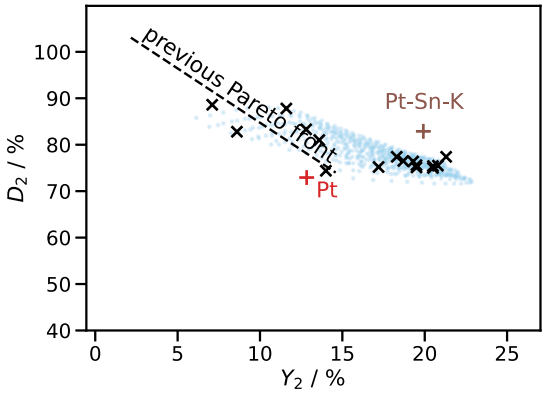

Figure 5. Overview over the rationally motivated (Pt, Mn, and Ca)-design space without surface-covering constraint. Performance descriptors for reaction yield Y_2 and deactivation D_2 for 607 unique catalysts in the design space as predicted by the regression model (blue dots). The descriptors for the explicitly measured compositions are shown as black crosses. Also shown are the descriptors for the unpromoted Pt catalyst (red cross), the Pt−Sn−K reference catalyst (brown cross), and the tentative Pareto front deduced before for surface-covering promotion, cf. Figure 2.

catalysts together with the predictions of the determined model for the entire design space. The models show a low root-mean-square error of 1.9 (1.9)% for Y_2 (D_2). As before, a Pareto front between the reaction yield and deactivation can clearly be discerned. However, confirming the expected support site contribution, this front is now shifted to higher Y_2. As a result, there are multiple promoter formulations with a predicted performance competitive to that of the equally not fully surface-covering Pt−Sn−K reference. In fact, when comparing the explicit reaction yield traces of the first and second PDH cycle shown in Figure 1 of one of such top-performing Pt−Mn−Ca catalysts that was part of the measurement batch, we even observe smaller conditioning effects. The Y_1 and D_1 of this catalyst are already almost the same as its Y_2 and D_2, whereas quite some reduction in both performance descriptors is observed between the first and second cycle for the Pt−Sn−K reference.

CONCLUSIONS

With less than a hundred experiments performed within a matter of weeks, we have identified a promising biopromoted Pt catalyst for the PDH that shows a performance in terms of reaction yield and deactivation resistance that is competitive to a Pt−Sn−K formulation as employed in the industrial Oleflex process. With a large-scale application in mind, this catalyst rests on a commercially available alumina support, an industrially viable Pt loading, and a simple synthesis protocol employing incipient wetness impregnation. The discovered Mn−Ca promotion demonstrates that there is nothing unique about the hitherto established Sn−K chemistry. In fact, while still showing a slightly inferior absolute performance, the new Pt−Mn−Ca system actually already exhibits a recovery after

https://doi.org/10.1021/acscatal.4c01740
ACS Catal. 2024, 14, 9008−9017

the first regeneration that is clearly better than that of the Pt−Sn−K reference. These findings constitute breakthroughs at the discovery stage. As is established practice throughout, this will now be followed by an optimization stage, where the compositions are fine-tuned, different synthesis routes leading to the same composition are explored (e.g., order of impregnation) and where it then makes sense to assess the longer-term stability over three and more cycles. There is little doubt that further performance gains will be achieved in this optimization stage, but such results might then no longer be published in the open literature.

However, even more remarkable than this discovery itself is in our view the way it was achieved. Initially, promoter action on catalyst performance was globally evaluated in a defined high-dimensional multipromoter space spanning six mindfully chosen promoters and suppressing additional support site effects through surface-covering promotion. This overview could be reached in a data- and time-efficient manner through careful experiment planning based on an iterative DoE approach utilizing space-filling algorithms and the development of a testing protocol for a multireactor setup that maximized the experimental throughput. Catalyst performance could quantitatively be compared through the definition of suitable yield and deactivation descriptors as well as stringently maintained reaction conditions. Following an insight-based iterative strategy, the obtained results motivated further analyses, which were supported by additional custom DoE designs and concomitant measurement batches. The observation of a Pareto front between yield and deactivation led to an effect analysis that traced the trade-off down to the individual promoter level, clearly identifying both positive and negative actions of the individual species. The resulting classification of the promoters into two groups with opposing actions on yield and deactivation led to an extension of the initial design space that revealed the most promising performance when reducing the total promoter number to ultimately one representative of each group. Abandoning the surface-covering promotion to also benefit from the intrinsic support site activity finally led to the global exploration of the low-dimensional (Pt, Mn, and Ca) design space that yielded the competitive formulation. Most importantly, the identification of this binary promoter search space was rationally achieved and is the result of the previous designs unraveling the synergistic action of this hardly reducible and one moderating element as well as the only insignificant interactions with the other promoters. Directly restricting the exploration to only binary promoter spaces would have implied assuming these insights and would hardly have reduced the experimental burden (at the present throughput capacity essentially by about 3 weeks).

This rational and systematic discovery approach stands in strong contrast to the scattered empirical catalysis literature, focusing on positive effects of individual promoters. The provided global understanding of trends, possibilities, and limitations in the multipromoter space is also much more than a mere global optimization as often strived for in closed-loop automated lab approaches.[48−54] Apart from enabling the efficient identification of promising multipromoter formulations, this understanding provides guidance on which systems would particularly merit deeper subsequent mechanistic studies and creates leads for insight-based modifications of the design space.

In contrast to widely known classic DoE, iterative DoE as pursued here should methodologically rather be seen as a highly data-efficient active-learning technique such as Bayesian optimization (BO). Like BO, it can query new experiments to refine the response model based on various optimality criteria. Able to robustly handle noise in the data and able to work with larger data batches, iterative DoE is in fact ideally suited for accelerated discovery within automated catalysis laboratories at present throughput capacities. Most importantly, and as demonstrated here, it can naturally deal with hypothesis- or insight-based adaptions of the design space between iterations. As such, it is in our view a far better suited approach to realize the human-in-the-loop paradigm of process automation. Based on the hitherto acquired data and knowledge, the involved human experts can make key decisions to suitably adapt the (otherwise automated) workflow for the next batch of experiments, rather than stoically executing an originally defined optimization in a fixed design space in a closed-loop setup.

METHODS

Synthesis. The catalysts were prepared in a home-built half automated setup by incipient wetness impregnation. Commercially available γ − alumina (BASF SE) with a particle size fraction of 300−500 μm was used as a support. Before impregnation, the support was thermally treated at 1000 °C for 12 h employing a heating rate of 5 °C min^{-1} and effectively achieving a phase transition to $\theta - Al_2O_3$. In a first step, 2 mL of different combinations of 2 M stock solutions of the metal precursors was then impregnated on 4 g of support using a dosing rate of 0.2 mL min^{-1}. The support was contained in a glass vessel, placed on a multisampling orbital shaker (Heidolph Instruments GmbH). The impregnated support was homogenized for 30 min at 1600 rpm. Using a multistage syringe pump (model Fusion 200-X, Chemyx Inc.), eight impregnations were performed in parallel. After that, the supported metal promoters were dried (2 h, 70 °C) and calcined (4 h, 500 °C, 10 °C min^{-1}) in a horizontal tubular furnace using 1 L min^{-1} of a mixture of 20% O_2 in He. In a second step, the catalysts were impregnated with an aqueous 85 mM solution of $Pt(NH_3)_4(NO_3)_2$ following the same procedure as described above. Finally, the catalysts were again dried (2 h, 70 °C) and calcined (2 h, 300 °C, 5 °C min^{-1}). After the thermal treatment, the furnace cooled down naturally. All reagents ($Fe(NO_3)_3 \cdot 9H_2O$ 99.9%, $Co(NO_3)_2 \cdot 6H_2O$ 99.9%, $Ca(NO_3)_2 \cdot 4H_2O$ 99.0%, $Ga(NO_3)_3 \cdot 8H_2O$ 98.0%, $K(NO_3)$ 99.0%, $Mn(NO_3)_2 \cdot 4H_2O$ 97.0%, and $Pt(NH_3)_4(NO_3)_2 \geq 50.0\%$ Pt) were obtained from Sigma-Aldrich and used as received without further purification. H_2O HPLC grade (Honeywell Riedel-de-Haën, Germany) was employed for the preparation of the metallic solutions.[55] As described in the main text, all catalyst preparations aim to achieve full total surface coverage. Based on results for Al[56] and extrapolating to the larger elements employed here, we estimate a surface concentration of 6 atoms/nm^2 to build a closed monolayer, cf. Supporting Information.

Catalytic Testing. The generation of catalytic performance data was conducted using an eight-fold parallel test setup equipped with gas dosing, reactor heating, and gas analysis units. Each of the prepared samples (500 mg, with the exact weight documented) was filled in a quartz tube reactor (d_{inner} = 3.8 mm) with a fixed bed embedded into a filling of steatite as the inert material. Above and below the catalytic bed, quartz

https://doi.org/10.1021/acscatal.4c01740
ACS Catal. 2024, 14, 9008−9017

wool was used to fix the bed heights within the reactor and ensure an isothermic temperature. The reactor temperatures were individually controlled and continuously monitored. The PDH reaction was run at 600 °C with a reactant gas flow comprising 10 mL min^{-1} propane, 5 mL min^{-1} hydrogen, and 2 mL min^{-1} nitrogen per reactor (WHSV = 2.4 $kg_{Propane}/h/kg_{Cat}$, GHSV = 720 $L_{Propane}/h/L_{Cat}$ or GHSV = 1224 $L_{feed}/h/L_{Cat}$).

Two PDH cycles were studied with a TOS of 24 h each. Prior to both reaction cycles, a reduction step was used as pretreatment of the catalyst at 600 °C for 1 h using 5 mL min^{-1} of hydrogen in 50 mL min^{-1}. Afterward, the reactors were cooled to 225 °C, which was determined as temperature with no observable catalytic activity. In between the two PDH cycles, a regeneration step was conducted using a stepped oxygen supply at a fixed temperature of 500 °C (5% O_2 and 20% O_2 using synthetic air diluted with nitrogen for 1 h each, heat-up with $\Delta T \approx 17$ K min^{-1} in regeneration stream). Before and after the catalytic test, as well as in between changing feed conditions, the samples were flushed with nitrogen. The analysis of the outlet gas stream was conducted using an online GC (GC 7890 A, Agilent) equipped with a flame ionization and a thermal conductivity detector for the identification and quantification of the reactants and reaction products like *n*-butane, 1-butene, propylene, ethane, ethylene, and methane. Besides, nitrogen was used as internal standard in the calculation of the gas compositions, in order to consider the gas expansion. In addition, the reactant gas composition was monitored continuously throughout the DoE using a bypass reactor. The test procedure was fully automated using the commercial software hte control; raw data evaluation was performed using the software tool myhte. The reproducibility of the catalytic test including the proof of independence of the sample placement throughout the eight reactors was given by performing reproduction experiments; see Figure S2 in the Supporting Information.

From the outlet concentrations (c_i), the propane conversion $X_{propane}$ and the selectivity S_i toward the quantified reaction products (i = propylene, ethane, ethylene, methane, butane, and butene) were calculated using a product based approach following eqs 2 and 3, with the number of carbon atoms represented by N_C.

$$X_{propane}\,[\%] = \left(1 - \frac{c_{propane}}{c_{propane} + \sum_{i=1}^{6}\left(c_i \cdot \frac{N_{C,i}}{3}\right)}\right) \cdot 100 \tag{2}$$

$$S_i\,[\%] = \frac{c_i \cdot N_{C,i}}{c_{propane} \cdot 3 + \sum_{i=1}^{6}(c_i \cdot N_{C,i})} \cdot 100 \tag{3}$$

From this, the yield $Y_{propylene}$ toward the desired product propylene is derived, combining the relative conversion of the hydrocarbon reactant and the selectivity to the olefin product

$$Y_{propylene}\,[\%] = X_{propane} \cdot \frac{c_{propylene}}{c_{propane} + \sum_{i=1}^{6}\left(c_i \cdot \frac{N_{C,i}}{3}\right)} \tag{4}$$

The strongly time-dependent $Y_{propylene}$ (t_{TOS}) are naturally given as a percentage of the constant amount of propane dosed per time. This molar flow rate of propane $r_{propane,in}$ into the reactor can be calculated from the employed volumetric flow rate $\dot{V}_{propane,in}$ and the molar volume at standard conditions V_m, cf. Supporting Information

$$r_{propane,in}\left[\frac{mmol}{h}\right] = \frac{\dot{V}_{propane,in}}{V_m} = \frac{10\left[\frac{mL}{min}\right] \cdot 60\left[\frac{min}{h}\right]}{1000\left[\frac{mL}{L}\right] \cdot 0.02241\left[\frac{L}{mmol}\right]} = 26.7\,\frac{mmol}{h} \tag{5}$$

The time-dependent molar flow rate of propylene then follows simply as

$$r_{propylene}(t_{TOS})\left[\frac{mmol}{h}\right] = Y_{propylene}(t_{TOS})\,[\%] \cdot r_{propane,in} \tag{6}$$

ASSOCIATED CONTENT

Supporting Information

The Supporting Information is available free of charge at https://pubs.acs.org/doi/10.1021/acscatal.4c01740.

Experimental details on synthesis and catalytic testing of the multipromoter and reference catalysts, experimental designs of the initial exploration and insight-guided extended design space, details on replication and reference catalysts, TRPT protocol, details of performance descriptors, regression models and their performance for the exploration of the multipromoter mixture design space and the Pt−Mn−Ca design space, exploration of the Pareto front, catalyst component effect along the Cox direction, and study workflow (PDF)

AUTHOR INFORMATION

Corresponding Authors

Frank Rosowski − *BasCat—UniCat BASF JointLab, Technische Universität Berlin, D-10623 Berlin, Germany; BASF SE, Catalysis Research, D-67065 Ludwigshafen, Germany*; Email: frank.rosowski@basf.com

Karsten Reuter − *Fritz-Haber-Institut der Max-Planck-Gesellschaft, D-14195 Berlin, Germany*; orcid.org/0000-0001-8473-8659; Email: reuter@fhi.mpg.de

Authors

Christian Kunkel − *Fritz-Haber-Institut der Max-Planck-Gesellschaft, D-14195 Berlin, Germany*

Frederik Rüther − *BasCat—UniCat BASF JointLab, Technische Universität Berlin, D-10623 Berlin, Germany*

Frederic Felsen − *Fritz-Haber-Institut der Max-Planck-Gesellschaft, D-14195 Berlin, Germany*

Charles W. P. Pare − *Fritz-Haber-Institut der Max-Planck-Gesellschaft, D-14195 Berlin, Germany*

Aybike Terzi − *BasCat—UniCat BASF JointLab, Technische Universität Berlin, D-10623 Berlin, Germany*

Robert Baumgarten − *BasCat—UniCat BASF JointLab, Technische Universität Berlin, D-10623 Berlin, Germany*

Esteban Gioria − *BasCat—UniCat BASF JointLab, Technische Universität Berlin, D-10623 Berlin, Germany*

https://doi.org/10.1021/acscatal.4c01740
ACS Catal. 2024, 14, 9008−9017

Raoul Naumann d'Alnoncourt − *BasCat—UniCat BASF JointLab, Technische Universität Berlin, D-10623 Berlin, Germany;* orcid.org/0000-0002-9946-4619
Christoph Scheurer − *Fritz-Haber-Institut der Max-Planck-Gesellschaft, D-14195 Berlin, Germany*

Complete contact information is available at: https://pubs.acs.org/10.1021/acscatal.4c01740

Author Contributions

C.K. and F.Rue. contributed equally. C.K., F.F., and C.S. designed the experiments. C.K. and C.P. curated data, analyzed, and conceptualized the results (if not otherwise stated). R.N.-d'A. and F.Rue. conceptualized the experimental TRPT strategy. F.Rue. and A.T. performed the catalytic measurements. F.Rue. conducted the literature search. R.B., E.G., and R.N.-d'A. conceptualized and carried out the synthesis. F.R., R.N.-d'A., C.S., and K.R. initially conceived the study. All authors contributed in conceptualizing the study. C.K., F.Rue., and K.R. wrote the manuscript.

Funding

Open access funded by Max Planck Society.

Notes

The authors declare no competing financial interest.

■ ACKNOWLEDGMENTS

This work was conducted in the framework of the BasCat—UniCat BASF JointLab between BASF SE, Technische Universität Berlin (TU Berlin), and Fritz-Haber-Institut (FHI) der Max-Planck-Gesellschaft. Funding by the Deutsche Forschungsgemeinschaft (DFG, German Research Foundation) under Germany's Excellence Strategy—EXC 2008−390540038—UniSysCat is acknowledged. We thank Abbas El-Jamal (TU Berlin) for diligent efforts and commitment in operating the synthesis setup and Jan Meißner (TU Berlin) for the technical support running the catalytic tests.

■ REFERENCES

(1) Pease, R. N.; Taylor, H. S. Promotor Action in Catalysis. *J. Phys. Chem.* **1920**, *24*, 241−265.
(2) Ertl, G. Elementary Steps in Heterogeneous Catalysis. *Angew. Chem., Int. Ed.* **1990**, *29*, 1219−1227.
(3) Hutchings, G. J. Promotion in Heterogeneous Catalysis: A Topic Requiring a New Approach? *Catal. Lett.* **2001**, *75*, 1−12.
(4) Schlögl, R. Heterogeneous Catalysis. *Angew. Chem., Int. Ed.* **2015**, *54*, 3465−3520.
(5) Han, Z.; Li, S.; Jiang, F.; Wang, T.; Ma, X.; Gong, J. Propane Dehydrogenation Over Pt−Cu Bimetallic Catalysts: The Nature of Coke Deposition and the Role of Copper. *Nanoscale* **2014**, *6*, 10000−10008.
(6) Wu, Z.; Bukowski, B. C.; Li, Z.; Milligan, C.; Zhou, L.; Ma, T.; Wu, Y.; Ren, Y.; Ribeiro, F. H.; Delgass, W. N.; Greeley, J.; Zhang, G.; Miller, J. T. Changes in Catalytic and Adsorptive Properties of 2 nm Pt_3Mn Nanoparticles by Subsurface Atoms. *J. Am. Chem. Soc.* **2018**, *140*, 14870−14877.
(7) Wegener, E. C.; Bukowski, B. C.; Yang, D.; Wu, Z.; Kropf, A. J.; Delgass, W. N.; Greeley, J.; Zhang, G.; Miller, J. T. Intermetallic Compounds as an Alternative to Single-atom Alloy Catalysts: Geometric and Electronic Structures from Advanced X-ray Spectroscopies and Computational Studies. *ChemCatChem* **2020**, *12*, 1325−1333.
(8) Cybulskis, V. J.; Bukowski, B. C.; Tseng, H.-T.; Gallagher, J. R.; Wu, Z.; Wegener, E.; Kropf, A. J.; Ravel, B.; Ribeiro, F. H.; Greeley, J.; Miller, J. T. Zinc Promotion of Platinum for Catalytic Light Alkane Dehydrogenation: Insights into Geometric and Electronic Effects. *ACS Catal.* **2017**, *7*, 4173−4181.
(9) Chen, S.; Pei, C.; Sun, G.; Zhao, Z.-J.; Gong, J. Nanostructured Catalysts toward Efficient Propane Dehydrogenation. *Acc. Mater. Res.* **2020**, *1*, 30−40.
(10) Zhang, Y.; Zhou, Y.; Shi, J.; Zhou, S.; Sheng, X.; Zhang, Z.; Xiang, S. Comparative Study of Bimetallic Pt-Sn Catalysts Supported on Different Supports for Propane Dehydrogenation. *J. Mol. Catal. A: Chem.* **2014**, *381*, 138−147.
(11) Carter, J. H.; Bere, T.; Pitchers, J. R.; Hewes, D. G.; Vandegehuchte, B. D.; Kiely, C. J.; Taylor, S. H.; Hutchings, G. J. Direct and Oxidative Dehydrogenation of Propane: From Catalyst Design to Industrial Application. *Green Chem.* **2021**, *23*, 9747−9799.
(12) Chen, S.; Chang, X.; Sun, G.; Zhang, T.; Xu, Y.; Wang, Y.; Pei, C.; Gong, J. Propane Dehydrogenation: Catalyst Development, New Chemistry, and Emerging Technologies. *Chem. Soc. Rev.* **2021**, *50*, 3315−3354.
(13) Sattler, J. J. H. B.; Ruiz-Martinez, J.; Santillan-Jimenez, E.; Weckhuysen, B. M. Catalytic Dehydrogenation of Light Alkanes on Metals and Metal Oxides. *Chem. Rev.* **2014**, *114*, 10613−10653.
(14) Araujo-Lopez, E.; Vandegehuchte, B. D.; Curulla-Ferré, D.; Sharapa, D. I.; Studt, F. Trends in the Activation of Light Alkanes on Transition-Metal Surfaces. *J. Phys. Chem. C* **2020**, *124*, 27503−27510.
(15) Werghi, B.; Wu, L.; Ebrahim, A. M.; Chi, M.; Ni, H.; Cargnello, M.; Bare, S. R. Selective Catalytic Behavior Induced by Crystal-Phase Transformation in Well-Defined Bimetallic Pt-Sn Nanocrystals. *Small* **2023**, *19*, 2207956.
(16) Shan, Y.; Hu, H.; Fan, X.; Zhao, Z. Recent Progress in Catalytic Dehydrogenation of Propane Over Pt-Based Catalysts. *Phys. Chem. Chem. Phys.* **2023**, *25*, 18609−18622.
(17) Burch, R. Platinum-Tin Reforming Catalysts: I. The Oxidation State of Tin and the Interaction Between Platinum and Tin. *J. Catal.* **1981**, *71*, 348−359.
(18) Bariås, O.; Holmen, A.; Blekkan, E.. In *Catalyst Deactivation 1994*; Delmon, B., Froment, G., Eds.; *Studies in Surface Science and Catalysis*; Elsevier, 1994; Vol. *88*; pp 519−524.
(19) Bariås, O. A.; Holmen, A.; Blekkan, E. A. Propane Dehydrogenation Over Supported Platinum Catalysts: Effect of Tin as a Promoter. *Catal. Today* **1995**, *24*, 361−364.
(20) Vladimir, H. Conversion of Hydrocarbons with Platinum Composite Catalyst. U.S. Patent 2,602,772 A, 1952.
(21) Zhang, Y.; Yao, W.; Fang, H.; Hu, A.; Huang, Z. Catalytic Alkane Dehydrogenations. *Sci. Bull.* **2015**, *60*, 1316−1331.
(22) Bhasin, M.; McCain, J.; Vora, B.; Imai, T.; Pujadó, P. Dehydrogenation and Oxydehydrogenation of Paraffins to Olefins. *Appl. Catal.* **2001**, *221*, 397−419.
(23) Nawaz, Z. Light Alkane Dehydrogenation to Light Olefin Technologies: A Comprehensive Review. *Rev. Chem. Eng.* **2015**, *31*, 413.
(24) Zhou, N.; Liu, W.; Jan, F.; Han, Z.; Li, B. Efficient Screening of Metal Promoters of Pt Catalysts for C−H Bond Activation in Propane Dehydrogenation from a Combined First-Principles Calculations and Machine-Learning Study. *ACS Omega* **2023**, *8*, 23982−23990.
(25) Ingale, P.; Knemeyer, K.; Preikschas, P.; Ye, M.; Geske, M.; Naumann d'Alnoncourt, R.; Thomas, A.; Rosowski, F. Design of PtZn Nanoalloy Catalysts for Propane Dehydrogenation Through Interface Tailoring via Atomic Layer Deposition. *Catal. Sci. Technol.* **2021**, *11*, 484−493.
(26) Docherty, S. R.; Rochlitz, L.; Payard, P.-A.; Copéret, C. Heterogeneous Alkane Dehydrogenation Catalysts Investigated via a Surface Organometallic Chemistry Approach. *Chem. Soc. Rev.* **2021**, *50*, 5806−5822.
(27) Van Assche, A.; Especel, C.; Le Valant, A.; Epron, F. Effect of Potassium and Platinum Contents on Catalytic Performance of Pt/Al_2O_3 Monometallic Catalysts for Propane Dehydrogenation. *Mol. Catal.* **2022**, *517*, 112059.
(28) Lee, M.-H.; Nagaraja, B. M.; Natarajan, P.; Truong, N. T.; Lee, K. Y.; Yoon, S.; Jung, K.-D. Effect of Potassium Addition on Bimetallic

PtSn/θ-Al_2O_3 Catalyst for Dehydrogenation of Propane to Propylene. *Res. Chem. Intermed.* **2016**, *42*, 123−140.
(29) Gao, X.-Q.; Yao, Z.-H.; Li, W.-C.; Deng, G.-M.; He, L.; Si, R.; Wang, J.-G.; Lu, A.-H. Calcium-Modified PtSn/Al_2O_3 Catalyst for Propane Dehydrogenation with High Activity and Stability. *ChemCatChem* **2023**, *15*, No. e202201691.
(30) Rimaz, S.; Chen, L.; Monzón, A.; Kawi, S.; Borgna, A. Enhanced Selectivity and Stability of Pt-Ge/Al_2O_3 Catalysts by Ca Promotion in Propane Dehydrogenation. *J. Chem. Eng.* **2021**, *405*, 126656.
(31) Cai, W.; Mu, R.; Zha, S.; Sun, G.; Chen, S.; Zhao, Z.-J.; Li, H.; Tian, H.; Tang, Y.; Tao, F. F.; Zeng, L.; Gong, J. Subsurface Catalysis-Mediated Selectivity of Dehydrogenation Reaction. *Sci. Adv.* **2018**, *4*, No. eaar5418.
(32) Liu, D.; Hu, H.; Yang, Y.; Cui, J.; Fan, X.; Zhao, Z.; Kong, L.; Xiao, X.; Xie, Z. Restructuring Effects of Pt and Fe in Pt/Fe-DMSN Catalysts and their Enhancement of Propane Dehydrogenation. *Catal. Today* **2022**, *402*, 161−171.
(33) Kwak, J. H.; Hu, J.; Mei, D.; Yi, C.-W.; Kim, D. H.; Peden, C. H. F.; Allard, L. F.; Szanyi, J. Coordinatively Unsaturated Al^{3+} Centers as Binding Sites for Active Catalyst Phases of Platinum on γ-Al_2O_3. *Science* **2009**, *325*, 1670−1673.
(34) Shi, L.; Deng, G.-M.; Li, W.-C.; Miao, S.; Wang, Q.-N.; Zhang, W.-P.; Lu, A.-H. Al_2O_3 Nanosheets Rich in Pentacoordinate Al^{3+} Ions Stabilize Pt-Sn Clusters for Propane Dehydrogenation. *Angew. Chem., Int. Ed.* **2015**, *54*, 13994−13998.
(35) Cesar, L. G.; Yang, C.; Lu, Z.; Ren, Y.; Zhang, G.; Miller, J. T. Identification of a Pt_3Co Surface Intermetallic Alloy in Pt−Co Propane Dehydrogenation Catalysts. *ACS Catal.* **2019**, *9*, 5231−5244.
(36) Rochlitz, L.; Pessemesse, Q.; Fischer, J. W. A.; Klose, D.; Clark, A. H.; Plodinec, M.; Jeschke, G.; Payard, P.-A.; Copéret, C. A Robust and Efficient Propane Dehydrogenation Catalyst from Unexpectedly Segregated Pt_2Mn Nanoparticles. *J. Am. Chem. Soc.* **2022**, *144*, 13384−13393.
(37) Fan, X.; Liu, D.; Sun, X.; Yu, X.; Li, D.; Yang, Y.; Liu, H.; Diao, J.; Xie, Z.; Kong, L.; Xiao, X.; Zhao, Z. Mn-Doping Induced Changes in Pt Dispersion and Pt_xMn_y Alloying Extent on Pt/Mn-DMSN Catalyst with Enhanced Propane Dehydrogenation Stability. *J. Catal.* **2020**, *389*, 450−460.
(38) Redekop, E. A.; Galvita, V. V.; Poelman, H.; Bliznuk, V.; Detavernier, C.; Marin, G. B. Delivering a Modifying Element to Metal Nanoparticles via Support: Pt−Ga Alloying during the Reduction of Pt/Mg(Al,Ga)O_x Catalysts and its Effects on Propane Dehydrogenation. *ACS Catal.* **2014**, *4*, 1812−1824.
(39) Sattler, J. J. H. B.; Gonzalez-Jimenez, I. D.; Luo, L.; Stears, B. A.; Malek, A.; Barton, D. G.; Kilos, B. A.; Kaminsky, M. P.; Verhoeven, T. W. G. M.; Koers, E. J.; Baldus, M.; Weckhuysen, B. M. Platinum-Promoted Ga/Al_2O_3 as Highly Active, Selective, and Stable Catalyst for the Dehydrogenation of Propane. *Angew. Chem., Int. Ed.* **2014**, *53*, 9251−9256.
(40) Searles, K.; Chan, K. W.; Mendes Burak, J. A.; Zemlyanov, D.; Safonova, O.; Copéret, C. Highly Productive Propane Dehydrogenation Catalyst Using Silica-Supported Ga−Pt Nanoparticles Generated from Single-Sites. *J. Am. Chem. Soc.* **2018**, *140*, 11674−11679.
(41) Siddiqi, G.; Sun, P.; Galvita, V.; Bell, A. T. Catalyst Performance of Novel Pt/Mg(Ga)(Al)O Catalysts for Alkane Dehydrogenation. *J. Catal.* **2010**, *274*, 200−206.
(42) Cornell, J.. In *Experiments with Mixtures: Designs, Models, and the Analysis of Mixture Data*; *Wiley Series in Probability and Statistics*; Wiley, 2002.
(43) Smith, W. *Experimental Design for Formulation; ASA-SIAM Series on Statistics and Applied Probability*; Society for Industrial and Applied Mathematics, 2005.
(44) Scheffé, H. Experiments with Mixtures. *J. R. Stat. Soc., B: Stat. Methodol.* **1958**, *20*, 344−360.
(45) Li, C.; Wang, G. Dehydrogenation of Light Alkanes to Mono-Olefins. *Chem. Soc. Rev.* **2021**, *50*, 4359−4381.
(46) Monai, M.; Gambino, M.; Wannakao, S.; Weckhuysen, B. M. Propane to Olefins Tandem Catalysis: A Selective Route Towards Light Olefins Production. *Chem. Soc. Rev.* **2021**, *50*, 11503−11529.
(47) Cox, D. R. A Note on Polynomial Response Functions for Mixtures. *Biometrika* **1971**, *58*, 155−159.
(48) Maier, W. F.; Stöwe, K.; Sieg, S. Combinatorial and High-Throughput Materials Science. *Angew. Chem., Int. Ed.* **2007**, *46*, 6016−6067.
(49) Potyrailo, R.; Rajan, K.; Stoewe, K.; Takeuchi, I.; Chisholm, B.; Lam, H. Combinatorial and High-Throughput Screening of Materials Libraries: Review of State of the Art. *ACS Comb. Sci.* **2011**, *13*, 579−633.
(50) Toyao, T.; Maeno, Z.; Takakusagi, S.; Kamachi, T.; Takigawa, I.; Shimizu, K.-i. Machine Learning for Catalysis Informatics: Recent Applications and Prospects. *ACS Catal.* **2020**, *10*, 2260−2297.
(51) Peng, J.; Schwalbe-Koda, D.; Akkiraju, K.; Xie, T.; Giordano, L.; Yu, Y.; Eom, C. J.; Lunger, J. R.; Zheng, D. J.; Rao, R. R.; Muy, S.; Grossman, J. C.; Reuter, K.; Gómez-Bombarelli, R.; Shao-Horn, Y. Human- and Machine-Centred Designs of Molecules and Materials for Sustainability and Decarbonization. *Nat. Rev. Mater.* **2022**, *7*, 991−1009.
(52) Margraf, J. T.; Jung, H.; Scheurer, C.; Reuter, K. Exploring Catalytic Reaction Networks with Machine Learning. *Nat. Catal.* **2023**, *6*, 112−121.
(53) Taniike, T.; Fujiwara, A.; Nakanowatari, S.; García-Escobar, F.; Takahashi, K. Automatic Feature Engineering for Catalyst Design Using Small Data without Prior Knowledge of Target Catalysis. *Commun. Chem.* **2024**, *7*, 11.
(54) Ramirez, A.; Lam, E.; Gutierrez, D. P.; Hou, Y.; Tribukait, H.; Roch, L. M.; Copéret, C.; Laveille, P. Accelerated Exploration of Heterogeneous CO_2 Hydrogenation Catalysts by Bayesian-Optimized High-Throughput and Automated Experimentation. *Chem Catal.* **2024**, *4*, 100888.
(55) Bariås, O. A.; Holmen, A.; Blekkan, E. A. Propane Dehydrogenation over Supported Pt and Pt−Sn Catalysts: Catalyst Preparation, Characterization, and Activity Measurements. *J. Catal.* **1996**, *158*, 1−12.
(56) Strempel, V. E.; Knemeyer, K.; Naumann d'Alnoncourt, R.; Driess, M.; Rosowski, F. Investigating the Trimethylaluminium/Water ALD Process on Mesoporous Silica by In Situ Gravimetric Monitoring. *Nanomaterials* **2018**, *8*, 365.

https://doi.org/10.1021/acscatal.4c01740
ACS Catal. 2024, 14, 9008−9017